Isothermal Crystallization and Melting Behaviors of Bionanocomposites from Poly(lactic acid) and TiO_2 Nanowires

Yonghui Li,[1] Caihong Chen,[2,3] Jun Li,[2] Xiuzhi Susan Sun[1]

[1]*Bio-Materials and Technology Lab, Department of Grain Science and Industry, Kansas State University, Manhattan, Kansas 66506*
[2]*Department of Chemistry, Kansas State University, Manhattan, Kansas 66506*
[3]*School of Chemistry and Chemical Engineering, South China University of Technology, Guangzhou 510640, People's Republic of China*

Received 24 February 2011; accepted 22 July 2011
DOI 10.1002/app.35326
Published online 3 November 2011 in Wiley Online Library (wileyonlinelibrary.com).

ABSTRACT: Two representative poly(lactic acid) (PLA) nanocomposites with 1% TiO_2 nanowires were prepared through *in situ* melt polycondensation and easy solution-mixing approaches, respectively. The former was denoted as ISPLANC, and the latter as SMPLANC. The isothermal crystallization kinetics and melting behaviors of pure PLA, ISPLANC, and SMPLANC were comparatively investigated by differential scanning calorimetry in the temperature range of 80–115°C. Maximum crystallization growth rate (G_{exp}) was observed at 100°C for all three samples. The well dispersed TiO_2 nanowires acted as effective nucleation agents in ISPLANC, which exhibited much higher G_{exp} in compared to pure PLA and SMPLANC below 110°C. However, much smaller crystallization enthalpy of ISPLANC was obtained because of its restricted chain mobility in forming crystalline lamellar. The crystallization behavior of all three samples fit the Avrami equation quite well, with most of the R^2 values larger than 0.9990. Double-melting behaviors were observed after heating the samples after isothermal crystallization at various temperatures, which was explained by the melt recrystallization of the smaller and imperfect crystals formed at lower isothermal crystallization temperatures. We also obtained the equilibrium melting temperatures of the three samples by carrying out Hoffman–Weeks plots. © 2011 Wiley Periodicals, Inc. J Appl Polym Sci 124: 2968–2977, 2012

Key words: poly(lactic acid) (PLA); TiO_2 nanowires; nanocomposites; differential scanning calorimetry (DSC); crystallization; melting behaviors

INTRODUCTION

Poly(lactic acid) (PLA) is a biodegradable polymer derived from renewable resources such as corn starch, sugar beets, cellulosic materials, etc. It is a most promising environmental-friendly thermoplastic that has potential applications in service utensils, packaging materials, appliance components, textiles, films, and biomedical materials.[1,2] In recent years, PLA nanocomposites have been intensively studied to improve PLA properties. Nanoparticles including carbon nanotubes, layered silicates or clays, and silica have been investigated widely to enhance the physical, thermal, and mechanical properties of pristine PLA.[3–7] PLA nanocomposites with nanoparticles such as graphite, polyhedral oligomeric silsesquioxane, TiO_2, MgO, hydroxyapatite, etc., also have been reported.[8–12]

In addition to the dispersion of nanoparticles in the PLA matrix and interfacial interaction between these two phases, the crystalline properties and melting behaviors of the PLA matrix and the effect of nanoparticles on them are of great importance for the properties and end use of PLA nanocomposites. For PLA and its nanocomposites prepared via melt polycondensation, a subsequent solid-state polymerization (SSP) is often necessary to increase further the molecular weight.[13–15] SSP process was usually conducted between the crystallization temperature and melting temperature of the polymer. The polymer tails and catalysts could be concentrated in the amorphous parts by the polymer crystallization to induce the molecular jump by polymer coupling.[14,15] Therefore, a thorough understanding of the crystallization kinetics and melting behaviors of PLA nanocomposites is crucial in the effort to optimize SSP process conditions and control of molecular weight of the final products. Additionally, control of crystallization factors allows for the design of polymeric materials with desirable properties.[16,17] The rate of

Correspondence to: X. S. Sun (xss@ksu.edu).
This article is Kansas Agricultural Experiment Station contribution 11-242-J.

Journal of Applied Polymer Science, Vol. 124, 2968–2977 (2012)

hydrolytic degradation of PLA also has been reported to be strongly affected by the degree of crystallinity.[18,19] Therefore, the crystalline lamellar organization of PLA plays an important role for controlling its degradation. Recent studies have examined the crystallization kinetics of PLA and its nanocomposites,[20–22] and the overall crystallization rate or crystallinity of PLA has been increased with the incorporation of various nanoparticles.[21–23]

In a previous study, we prepared PLA nanocomposites with TiO_2 nanowires through an *in situ* melt polycondensation approach.[24] PLA chains were covalently bonded to the nanowire surface through the bidentate coordination between Ti atoms and the carboxyl groups of lactic acid, and the resultant nanocomposites showed a satisfactory dispersion of nanowires and interfacial interaction. Significantly improved glass transition temperature and thermal stability were observed for the bonded PLA chains.[24] In this study, we will report the isothermal crystallization kinetics and melting behaviors of such nanocomposites and pure PLA. For comparison purposes, the nanocomposites prepared by easy solution-mixing of PLA and TiO_2 nanowires also were studied and reported.

EXPERIMENTAL

Materials

TiO_2 nanowires were synthesized in our lab following previously described procedures.[25] Briefly, 0.1 g TiO_2 nanopowders were placed into a Teflon-lined autoclave of 50 mL capacity. It was then filled with 40 mL 10*M* NaOH aqueous solution, sealed into a stainless steel tank and maintained at 200°C for 24 h without stirring. After cooling down, the sample was washed with 1*M* aqueous HCl solution, deionized water, and absolute ethanol several times and dried at 80°C for 12 h. Finally, we obtained soft fibrous TiO_2 nanowires with white color. Pure PLA and *in situ* polymerized PLA/1% TiO_2 nanowire nanocomposites were prepared via melt polycondensation of L-lactic acid without and with TiO_2 nanowires, respectively, as reported previously.[24] A determined amount of TiO_2 nanowires were added to a 90 wt % aqueous solution of L-lactic acid and ultrasonically treated for 30 min. The mixture was first subjected to a dehydration/oligomerization process at 110–150°C for 9 h at reduced pressure, and then melt polycondensation was conducted at 180°C for 10 h at 10 Torr with $SnCl_2 \cdot H_2O$ and *p*-toluenesulfonic acid monohydrate as binary catalysts. The weight-average molecular weights of the pure PLA and the nanocomposites were 63,000 and 66,000 (based on polystyrene standard), respectively, with polydispersity of about 2. Chloroform was purchased from Fisher Scientific.

Preparation of nanocomposite films

The solution-mixing PLA/1% TiO_2 nanowire nanocomposites were prepared by using the solution-intercalation film-casting technique as follows: 0.02 g of TiO_2 nanowires was added to 20 mL chloroform, and the mixture was sonicated for 30 min to achieve a uniform dispersion. Meanwhile, 2 g of synthesized pure PLA was completely dissolved in 20 mL chloroform. The PLA solution and nanowire dispersion were stirred for 1 h and sonicated for 1 h. The mixture was cast on a Petri dish at room temperature, kept in a fume hood with controlled evaporation of the solvent for 1 week, then dried in a vacuum oven for 24 h at 80°C to evaporate any residual solvent. Eventually, the solution-mixing nanocomposite (SMPLANC) film was obtained. Pure PLA and *in situ* polymerized nanocomposites (ISPLANC) also were dissolved in chloroform, and films were obtained similarly. The crystallization and melting behaviors of these three types of samples (PLA, ISPLANC, and SMPLANC) were compared. All the samples for microscopy and crystallization studies were cut from these cast films.

Optical microscopy

The dispersion of TiO_2 nanowires in the ISPLANC and SMPLANC films was examined with an Olympus BX50 microscope. The images were captured with a Nikon Digital Camera DXM 1200F using Nikon ACT-1 version 2.62 software.

Differential scanning calorimetry analysis

The isothermal crystallization and melting behaviors of PLA, ISPLANC, and SMPLANC were studied with a TA differential scanning calorimetry (DSC) Q200 instrument under a nitrogen atmosphere. The DSC instrument was calibrated using the melting temperature and enthalpy of indium. The sample films were weighed (around 8 mg) in a standard aluminum pan and sealed. An empty sealed pan was used as a reference. For crystallization characterization, a sample was heated from 0 to 190°C at a rate of 10 °C/min, and maintained at 190°C for 5 min. Subsequently, it was rapidly cooled ($\sim$ 60 °C/min) to the isothermal crystallization temperature (T_c). T_c for the samples ranged from 80 to 115°C at 5°C intervals; samples were held at each T_c for 30–50 min, allowing complete crystallization. To observe melting behavior, the completely crystallized sample was reheated from T_c to 190°C at a rate of 10 °C/min. Heat of melting (ΔH_m) and melting temperature

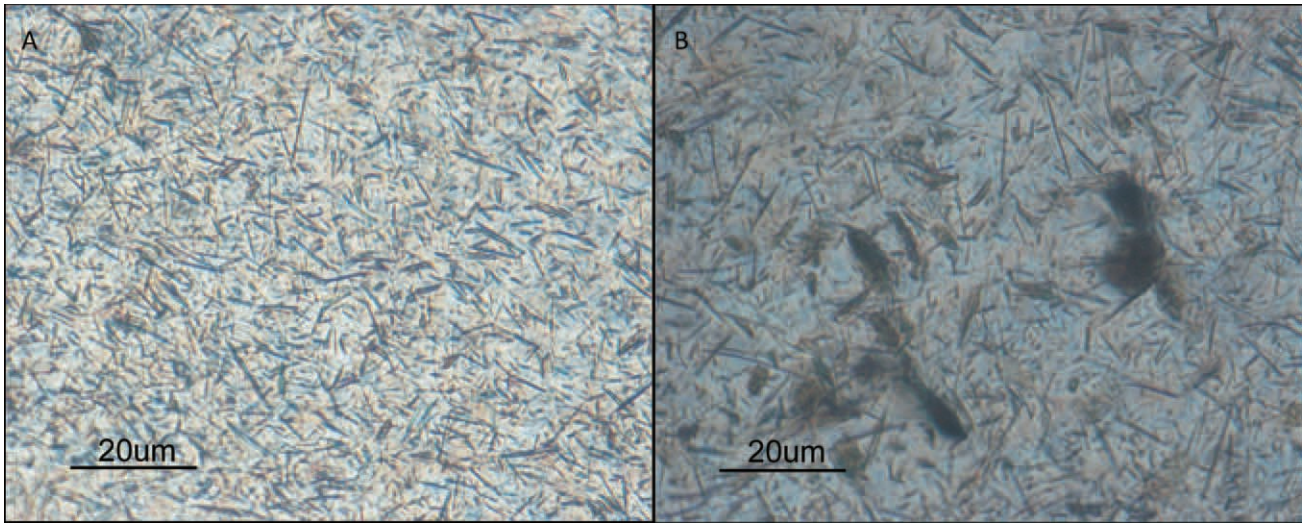

Figure 1 Microscope images of PLA nanocomposite films (A: ISPLANC; B: SMPLANC). [Color figure can be viewed in the online issue, which is available at wileyonlinelibrary.com.]

(T_m) were determined from the DSC thermograms. Crystallinity (X_m) was estimated according to the following eq. (1):

$$X_m = \frac{\Delta H_m}{\Delta H_0 \times X_{\mathrm{PLA}}} \tag{1}$$

where ΔH_m and ΔH_0 are heats of melting (J/g) of the measured sample and of PLA crystals of infinite size with a value of 93.6 J/g,[26] respectively, and X_{PLA} is the PLA fraction in the sample ($X_{\mathrm{PLA}} = 1$ for PLA, and $X_{\mathrm{PLA}} = 0.99$ for ISPLANC and SMPLANC).

RESULTS AND DISCUSSION

Morphology

The image of synthesized TiO_2 nanowires was reported in our previous article.[24] The diameter was $\sim$ 50–200 nm and length from a few micrometers to $\sim$ 20 μm. Figure 1 shows the microscopy images of ISPLANC (A) and SMPLANC (B) films. No nanowire aggregate was observed for ISPLANC film. The individual nanowires were distributed homogeneously throughout the polymer matrix, indicating that *in situ* polymerization was an effective approach to achieve nanocomposites with uniform distributions. Because of the ease of dispersion of TiO_2 nanowires in the aqueous L-lactic acid monomer and *in situ* grafting of lactic acid oligomer on to the surface of nanowires, the nanowires could be well dispersed in the PLA matrix. However, for the nanocomposites prepared by easy solution-mixing of PLA and TiO_2 nanowires (SMPLANC), severe aggregation of TiO_2 nanowires occurred because of the hydrophilic nature and high surface area of nanowires.

Isothermal crystallization behavior

Figure 2(A–C) shows the DSC thermograms of PLA, ISPLANC, and SMPLANC at T_c's from 80 to 115°C. Generally, the T_c is chosen in the range between the glass transition temperature (T_g) and equilibrium melting temperature (T_m^0), at which temperature polymer can crystallize. The T_m^0 will be discussed in the next section. When the melted semicrystalline polymer is cooled down and maintained at T_c, its crystallization rate depends on its degree of supercooling (i.e., $\Delta T = T_m^0 - T_c$).[27] Shortest crystallization peak time was noticed at T_c of 100°C for all the samples. Upon increasing or decreasing T_c beyond 100°C in the investigated temperature range, the isothermal crystallization peaks became broader; therefore, the time required for the complete crystallization became longer. Furthermore, ISPLANC exhibited a much narrower crystallization peak with lower peak position at each T_c compared with pure PLA and SMPLANC, which will be discussed later as crystallization half-time and crystallization growth rate.

Based on the samples' DSC exotherms in terms of the heat flow per gram of the sample (dH/dt) as a function of crystallization time, t, we plotted the relative crystallinity, $\alpha(t)$, as a function of t (Fig. 3A–C). The relative crystallinity is defined as follows:

$$\alpha(t) = \frac{\Delta H(t)}{\Delta H_\infty} \tag{2}$$

where $\Delta H(t)$ is the enthalpy of isothermal crystallization at time t [eq. (3)] and ΔH_∞ is the value after complete crystallization [eq. (4)]. In this study, ΔH_∞ is the total area under the crystallization curve, as listed in Table I.

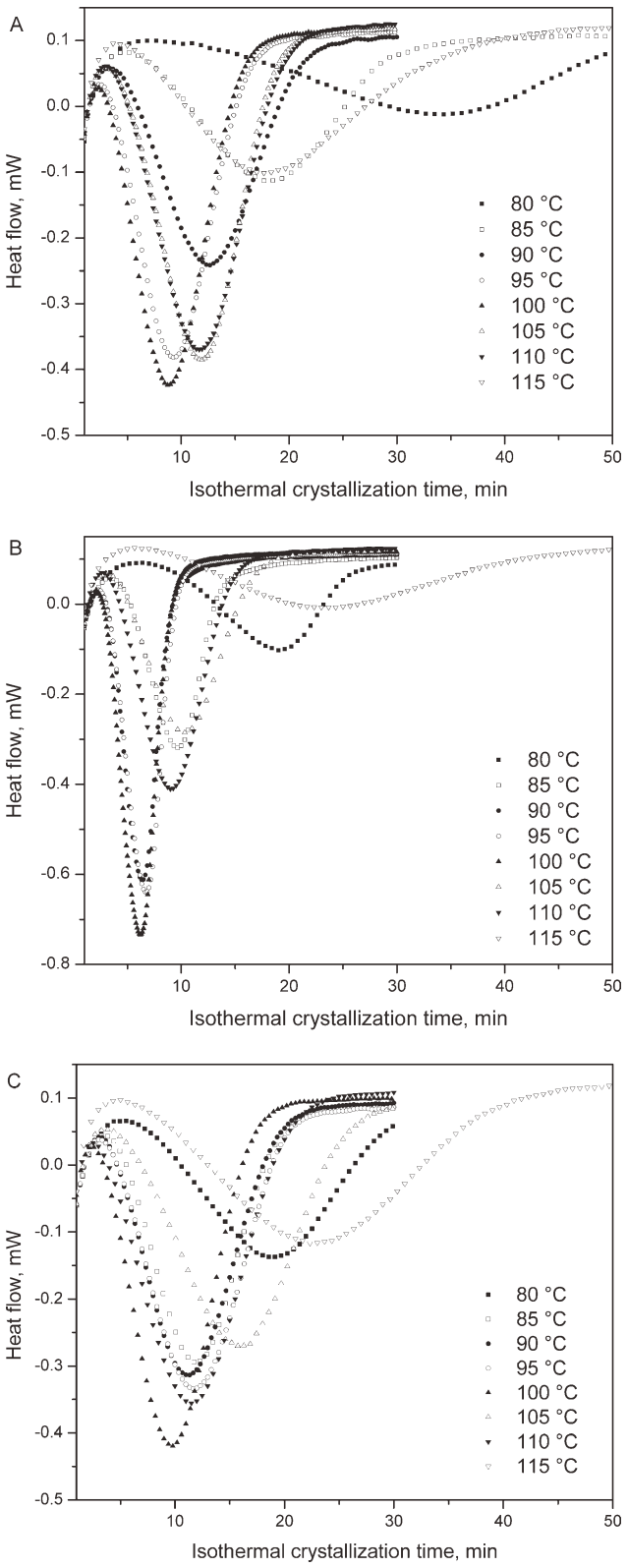

Figure 2 Isothermal crystallization thermograms of PLA (A) and its nanocomposites (B: ISPLANC; C: SMPLANC) at various temperatures.

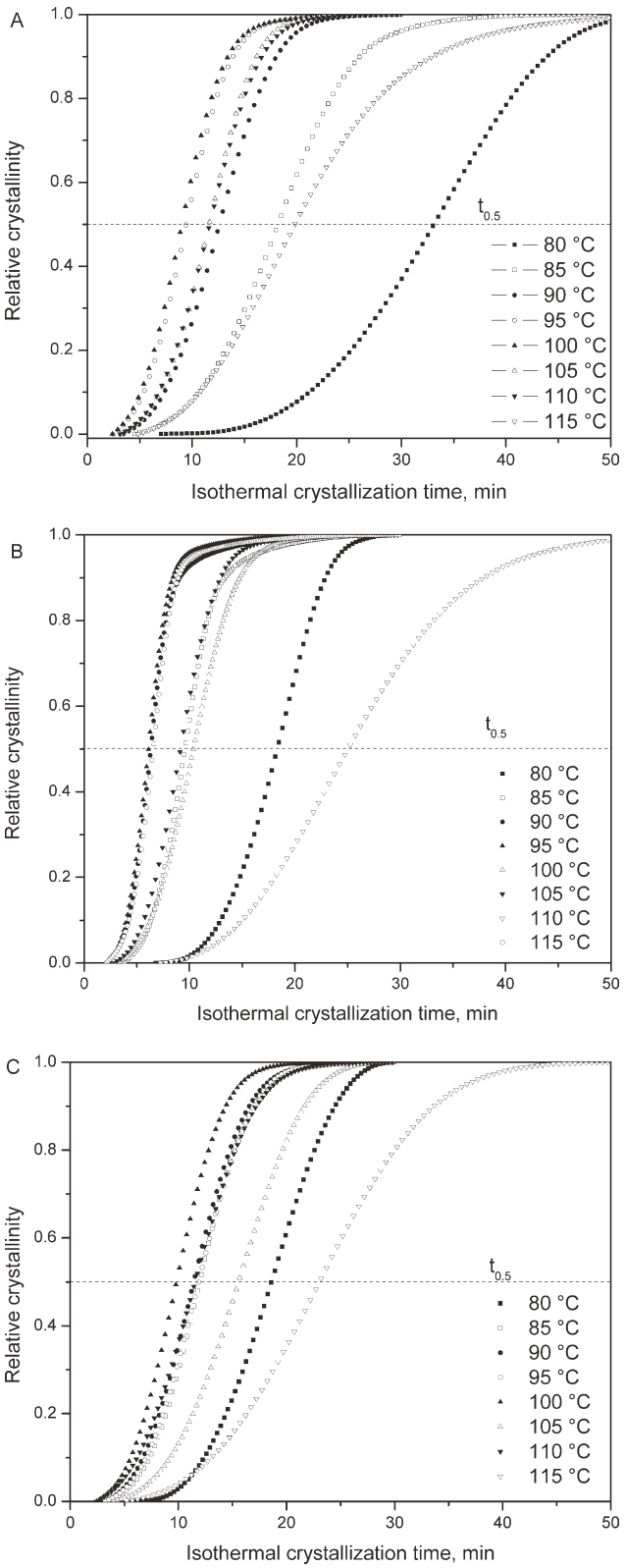

Figure 3 Relative crystallinity as a function of isothermal crystallization time for PLA (A) and its nanocomposites (B: ISPLANC; C: SMPLANC) at various temperatures.

TABLE I
Summary of Isothermal Crystallization Data of PLA and its Nanocomposites (ISPLANC and SMPLANC)

Sample	T_c (°C)	ΔH_∞ (J/g)	$t_{0.5exp}$ (min)	G_{exp} (min^{-1})	K (min^{-1})	n	n_{ave}	R^2	$t_{0.5cal}$ (min)	G_{cal} (min^{-1})
PLA	80	23.9	33.1	3.02E−02	1.97E−07	4.31	3.52	0.9992	33.0	3.03E−02
	85	25.5	18.2	5.49E−02	2.35E−05	3.54		0.9999	18.3	5.46E−02
	90	28.1	12.6	7.92E−02	9.33E−05	3.51		0.9998	12.7	7.89E−02
	95	30.6	9.5	1.06E−01	3.82E−04	3.34		0.9999	9.5	1.06E−01
	100	32.5	9.0	1.11E−01	4.95E−04	3.29		0.9997	9.0	1.11E−01
	105	36.1	11.6	8.59E−02	8.96E−05	3.65		0.9999	11.6	8.60E−02
	110	37.7	11.7	8.55E−02	1.27E−04	3.50		0.9999	11.7	8.56E−02
	115	32.8	19.8	5.05E−02	8.27E−05	3.01		0.9965	20.1	4.97E−02
ISPLANC	80	14.3	18.3	5.46E−02	6.24E−08	5.58	4.34	0.9982	18.3	5.46E−02
	85	15.6	9.6	1.04E−01	2.10E−05	4.60		0.9992	9.6	1.04E−01
	90	17.2	6.3	1.58E−01	1.92E−04	4.43		0.9997	6.4	1.57E−01
	95	19.5	6.6	1.53E−01	2.10E−04	4.31		0.9999	6.6	1.53E−01
	100	21.6	6.1	1.64E−01	2.29E−04	4.43		0.9995	6.1	1.64E−01
	105	21.0	10.4	9.64E−02	1.00E−04	3.78		0.9992	10.4	9.64E−02
	110	24.2	9.2	1.09E−01	1.14E−04	3.93		0.9992	9.2	1.09E−01
	115	26.2	25.1	3.99E−02	5.56E−06	3.63		0.9942	25.3	3.95E−02
SMPLANC	80	21.0	19.0	5.26E−02	7.37E−07	4.70	3.62	0.9971	18.7	5.36E−02
	85	25.2	12.0	8.35E−02	5.27E−05	3.82		0.9997	12.0	8.35E−02
	90	28.0	11.4	8.75E−02	1.20E−04	3.55		0.9993	11.5	8.71E−02
	95	30.4	11.9	8.41E−02	1.03E−04	3.56		0.9995	11.9	8.41E−02
	100	31.6	9.8	1.02E−01	3.35E−04	3.34		0.9998	9.8	1.02E−01
	105	33.4	15.6	6.42E−02	3.26E−05	3.63		0.9999	15.6	6.43E−02
	110	34.8	11.6	8.65E−02	4.26E−04	3.02		0.9999	11.6	8.65E−02
	115	35.8	23.1	4.34E−02	2.04E−05	3.32		0.9998	23.2	4.32E−02

$$\Delta H(t) = \int_0^t \left(\frac{dH}{dt}\right) dt \quad (3)$$

$$\Delta H_\infty = \int_0^\infty \left(\frac{dH}{dt}\right) dt \quad (4)$$

All the $\alpha(t)$ versus t plots exhibited similar sigmoidal profiles. A relevant kinetic characterization, obtained by the intersection of the $\alpha(t)$ versus t plots and the horizontal line at $\alpha(t) = 0.5$, as shown in Figure 3(A–C), is the experimental crystallization half-time ($t_{0.5exp}$). The $t_{0.5exp}$ corresponds to the time necessary for the sample to reach 50% of its maximum crystallinity. The reciprocal value of $t_{0.5\ exp}$ is assumed to be equal to the experimental crystallization growth rate (G_{exp}). Table I summarizes the $t_{0.5exp}$ and G_{exp} values as derived from Figure 3. The change of G_{exp} as a function of T_c was plotted in Figure 4 to provide a better visualization. Increasing the crystallization temperature for each sample initially caused G_{exp} values to increase and then to decrease. Such behavior is common for polymers due to the balance between two opposing effects on the crystallization.[28] As T_c decreases and approaches T_g, the crystallization growth rate is greatly retarded by the significant decrease in chain mobility. When T_c increases and approaches the T_m^0, although chain mobility increases, it is overcome by the great decrease of the formed nucleation density, and the crystallization growth rate decreases at low degrees of supercooling (i.e., smaller ΔT).

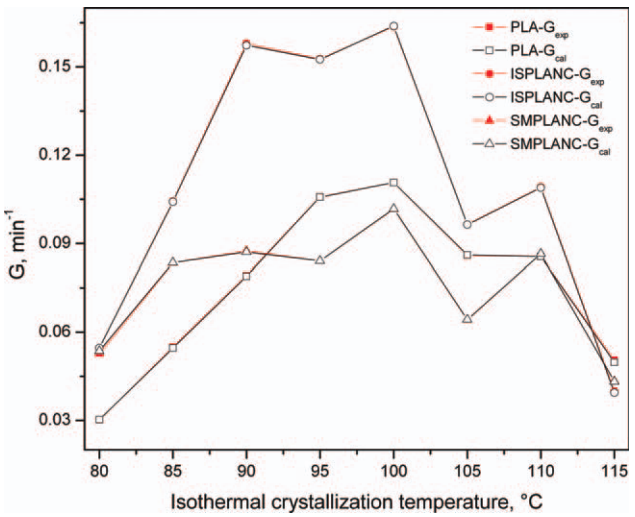

Figure 4 Experimental (G_{exp}) and calculated (G_{cal}) crystallization rate of PLA and its nanocomposites (ISPLANC and SMPLANC) as a function of temperatures. [Color figure can be viewed in the online issue, which is available at wileyonlinelibrary.com.]

The minimum $t_{0.5\ exp}$ was observed at 100°C for both PLA and nanocomposites, with $t_{0.5exp}$ of 9.0 min and G_{exp} of 0.11 min^{-1} for PLA, $t_{0.5exp}$ of 6.1 min and G_{exp} of 0.16 min^{-1} for ISPLANC, and $t_{0.5exp}$ of 9.8 and G_{exp} of 0.10 min^{-1} for SMPLANC. The G_{exp} of ISPLANC was much higher than that of pure PLA at T_c below 110°C because of the nucleation effects of TiO_2 nanowires. At T_c above 110°C, the G_{exp} of ISPLANC decreased faster than that of

pure PLA; at 115°C it was even lower. This can be explained by its much lower T_m^0 (161.7°C) than that of pure PLA (188.4°C). At the same T_c, the ISPLANC system was subjected to more decrease of formed nucleation density because of its lower degree of supercooling than pure PLA. As a result, its crystallization growth rate decreased.

The G_{exp} of SMPLANC was larger than that of pure PLA at T_c of 90°C and below, but smaller at T_c of 95°C and above. Polymer crystallization generally involves nucleation and crystalline growth processes. At lower T_c, the TiO_2 nanowires acted as additional nucleation sites in the SMPLANC system compared with pure PLA, and nucleation was the dominant factor in determining the G_{exp}. While at higher T_c, due to the high concentration and poor dispersion of nanowires in the SMPLANC system, the mobility of PLA chains was restricted and the crystalline growth process was retarded. Furthermore, the effect of TiO_2 nanowires on PLA crystallization in SMPLANC system was much less obvious than that in ISPLANC system. The nanocomposites prepared through solution mixing did not have strong interfacial interaction between PLA matrix and TiO_2 nanowires, and the dispersion of TiO_2 nanowires was not satisfying. Therefore, the effect of TiO_2 nanowires on the crystallization of surrounding PLA chains for SMPLANC became less significant. Although ISPLANC crystallized more rapidly than pure PLA and SMPLANC, its crystallization enthalpy (ΔH_∞) was much smaller at each T_c (Table I) because of its restricted chain mobility in forming crystalline lamellar.

Avrami analysis is the most popular and easiest methodology to achieve relevant parameters for characterizing the crystallization kinetics of polymers.[29] The fundamental Avrami equation [eq. (5)] below was used to analyze the increase of the relative crystallinity with time[30–32]:

$$\alpha(t) = 1 - \exp(-kt^n) \tag{5}$$

where k is the Avrami rate constant and n is the Avrami exponent. The values of k and n are diagnostic of the crystallization mechanism. They are related to the crystallization half-time and to the type of nucleation together with the geometry of the crystal growth, respectively.

Applying the natural logarithmic properties to both sides of eq. (5), obtains the following equation:

$$\ln(-\ln(1-\alpha(t))) = \ln(k) + n\ln(t) \tag{6}$$

This equation was used to construct the Avrami fit plots as shown in Figure 5(A–C) to calculate the k and n. The experimental data was also drawn as scatter plots in Figure 5(A–C). Because the Avrami equation rarely describes the whole conversion

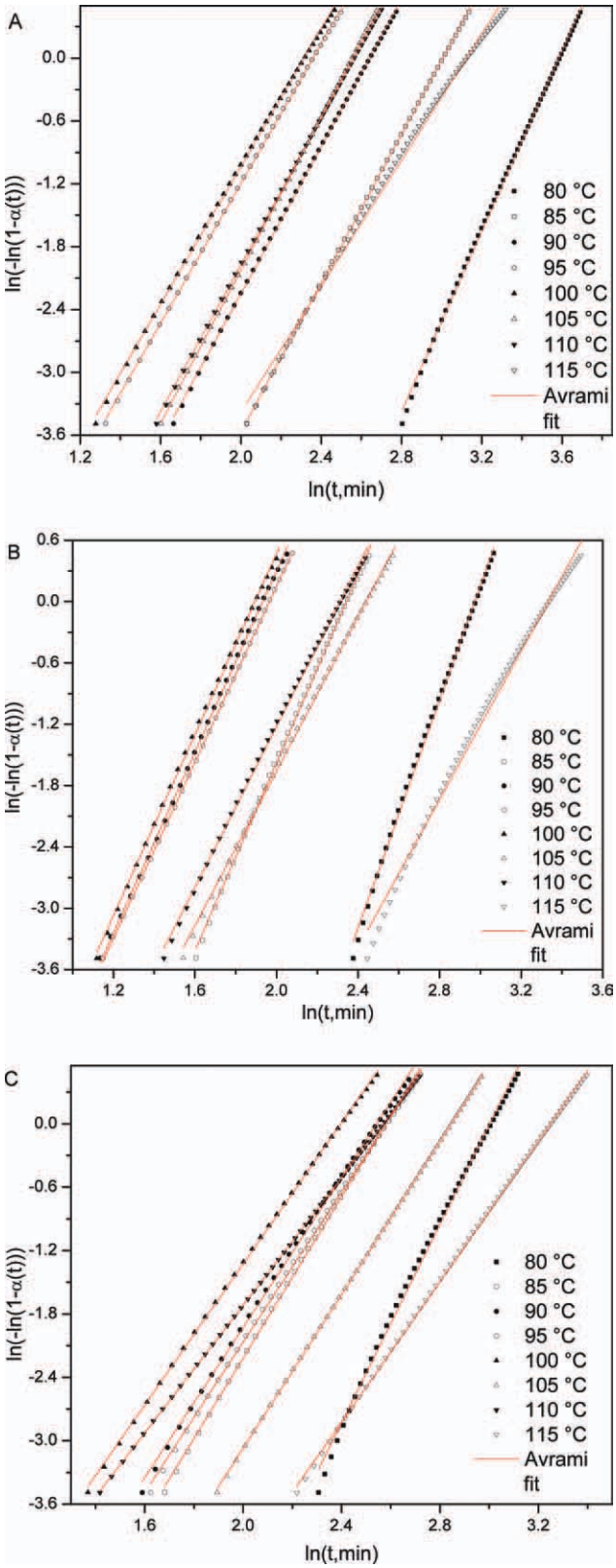

Figure 5 Avrami analysis of the isothermal crystallization data of PLA (A) and its nanocomposites (B: ISPLANC; C: SMPLANC) at various temperatures. [Color figure can be viewed in the online issue, which is available at wileyonlinelibrary.com.]

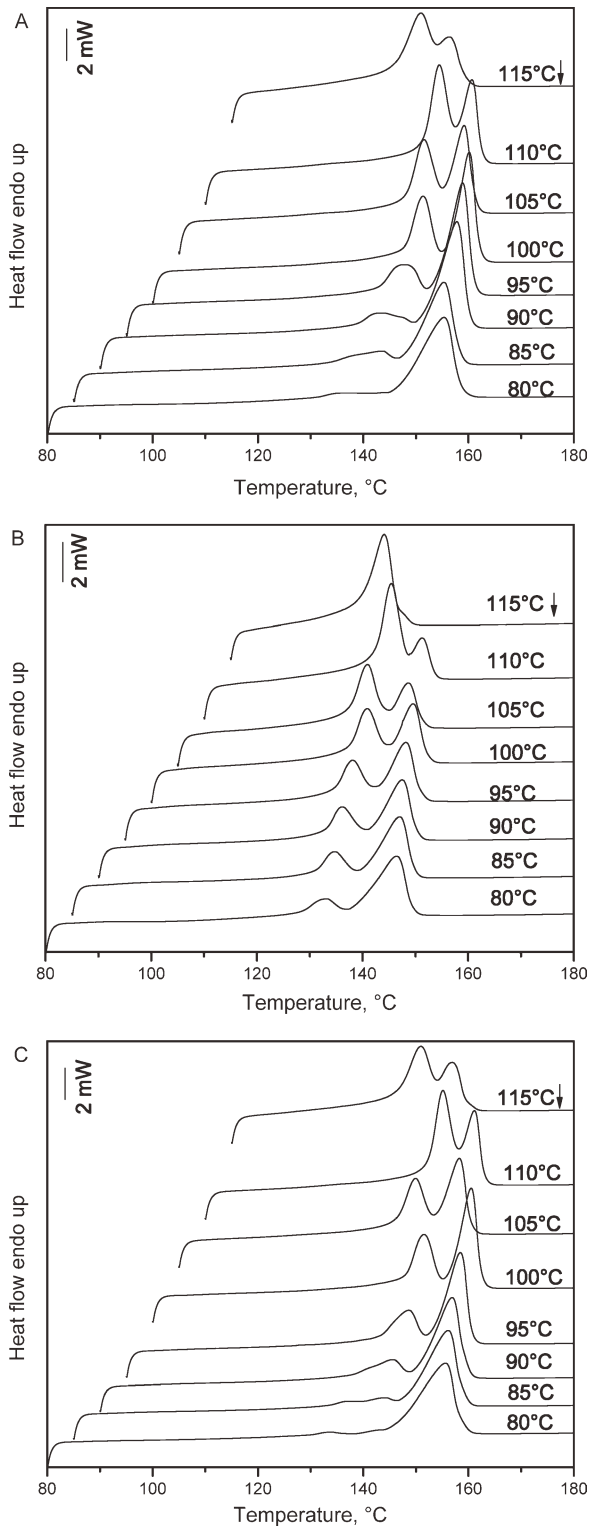

Figure 6 DSC melting thermograms of PLA (A) and its nanocomposites (B: ISPLANC; C: SMPLANC) after isothermal crystallization at various temperatures.

process, we drawn only the plots for $\alpha(t)$ from 0.03 to 0.8 based on the literature.[33] If the experimental data obey the Avrami theory, the Avrami fitting lines should fit the experimental data quite well, yielding $\ln(k)$ as an intercept and n as a slope. The Avrami constants k and n and correlation coefficient of the fit R^2 were summarized in Table I. Most of the R^2 values were larger than 0.9990, indicating a very good Avrami fit of the data.[33]

The Avrami exponent n differed from sample to sample, and it also varied with T_c. The average n value of 3.5–3.6 in the T_c range evaluated for PLA and SMPLANC indicated that the crystal growing mechanism was intermediate between the instantaneous ($n = 3$) and sporadic ($n = 4$) types of nucleation, and the growing of spherulites was three-dimentional.[16] The average n value of ISPLANC was 4.3, which can be theoretically explained by the introduction of a nucleation index m ($m = n - 4$).[29] The values of m between 0 and 1 indicated that the nature of the nucleation rate increased with time with sporadic nucleation mechanism during crystallization process. The n values can be affected by many factors, such as the mechanism of nucleation, nucleation density, the form of crystalline growth, restriction of crystalline formation due to surrounding fillers, and even the detecting techniques used. PLA n values in the range of 2–5.4 have been reported.[16,34–36] The rate constant k is determined by the balance of two factors, the rate of nucleation and the crystalline growth. The former increases with supercooling, but the latter decreases; consequently, a maximum value of k exists at a given supercooling. As shown in Table I, for all the samples, the k values first increased as T_c increased and then decreased generally, similar to the tendency of G_{exp}.

To further confirm whether the crystallization of PLA and nanocomposites follows the Avrami model, the crystallization half-time values also were calculated from the knowledge on k and n as follows[27]:

$$G_{cal} = \frac{1}{t_{0.5cal}} = \frac{1}{\left(\frac{\ln 2}{k}\right)^{\frac{1}{n}}}$$

where $t_{0.5cal}$ is the calculated crystallization half-time and G_{cal} is the calculated crystallization rate, which are shown in Table I. Figure 4 illustrates the comparison between the isothermal crystallization rate as calculated from the Avrami parameters and the same kinetic parameter as directly derived from the experimental relative crystallinity data. The agreement observed between the two series of data revealed that the crystallization kinetics of all the samples followed the Avrami model.

Melting behaviors

The melting thermograms of PLA and its nanocomposites (ISPLANC and SMPLANC) after isothermal crystallization at various T_c's are presented in Figure 6(A–C), and the data are summarized in Table II. All

TABLE II
Melting Parameters of PLA and its Nanocomposites (ISPLANC and SMPLANC) Derived from DSC Melting Thermograms After Isothermal Crystallization at Various Temperatures

Sample	T_c (°C)	T_m(L) (°C)	T_m(H) (°C)	ΔH_m (J/g)	X_m
PLA	80	135.8	155.4	36.6	0.39
	85	143.1	155.3	37.2	0.40
	90	143.1	157.8	40.4	0.43
	95	147.2	158.9	41.9	0.45
	100	151.2	160.2	43.3	0.46
	105	151.4	159.2	43.7	0.47
	110	154.4	160.7	45.8	0.49
	115	150.9	156.4	43.9	0.47
ISPLANC	80	133.3	146.4	20.2	0.22
	85	134.4	147.0	21.4	0.23
	90	136.2	147.5	22.0	0.24
	95	137.9	148.2	23.5	0.25
	100	141.0	149.6	25.1	0.27
	105	140.9	148.7	23.9	0.26
	110	145.4	151.3	27.5	0.30
	115	144.1	144.1	30.5	0.33
SMPLANC	80	134.6	155.6	35.5	0.38
	85	143.5	156.2	35.5	0.38
	90	145.7	156.9	36.9	0.40
	95	148.5	158.4	39.1	0.42
	100	151.5	160.5	41.8	0.45
	105	150.0	158.2	40.0	0.43
	110	155.2	161.1	45.5	0.49
	115	150.9	156.9	40.9	0.44

the samples exhibited double-melting behaviors, except for ISPLANC after isothermal crystallization at T_c of 115°C. L and H are used for the names of the low-temperature and high-temperature melting peaks. On the basis of this notation, the peak melting temperatures of L and H are denoted as T_m(L) and T_m(H), respectively. For both PLA and nanocomposites, the area of L increased with increasing T_c, whereas the area of H decreased. In other words, the ratio of peak area of H to that of L was dependent on T_c, which could be explained by the melt-recrystallization model.[37,38] The melt-recrystallization model suggests that small and imperfect crystals change successively into more stable crystals through the melt-recrystallization mechanism. That is, the melting and recrystallization are competitive in the heating process.[38] When the samples were crystallized at lower T_c's, the mobility of polymer chains was restricted, resulting in smaller crystallite structures and more defect-ridden crystalline lamellar. Such crystals recrystallized in the melt-recrystallization process during heating, leading to a higher melting peak. While at higher T_c's, forming more perfect and larger crystal lamellae were easier, and therefore it was more difficult for the recrystallization process to occur. As a result, the area of peak H became smaller or even disappeared for the samples crystallized at higher T_c. In summary, peak H is a result of the melting of the crystallites recrystallized during the heating process, whereas peak L refers to the melting of the primary crystallites formed during the isothermal crystallization process.

As shown in Table II, the heat of melting (ΔH_m) and crystallinity (X_m) of PLA and nanocomposites also are affected by T_c. The X_m of PLA and nanocomposites increased in general as the T_c increased in the evaluated temperature range. This is because additional crystallization occurred during isothermal crystallization at higher T_c, corresponding to the higher ΔH_∞ as reported in Table I. The much lower X_m in the ISPLANC compared with pure PLA was due to the inability of polymer chains to be incorporated fully into growing crystalline lamella. In other words, the presence of high concentrations of dispersed TiO_2 nanowires and strong covalent bonding between nanowire surface and PLA chains prevented large crystalline domains from forming due to limited space and restricted mobility imposed on PLA chains. SMPLANC also exhibited lower X_m compared with pure PLA, but to a much smaller extent than ISPLANC. As expected, the nanocomposites prepared through solution mixing did not have strong interfacial interaction between PLA matrix and TiO_2 nanowires. Because of the lack of efficient interfacial interaction and homogeneous dispersion of nanowires, the effect of nanowires on the mobility of PLA chains in forming crystalline lamellar was expected to be much smaller compared with ISPLANC. Decreased crystallinity also was reported for other PLA nanocomposites in the literature.[6,11,17]

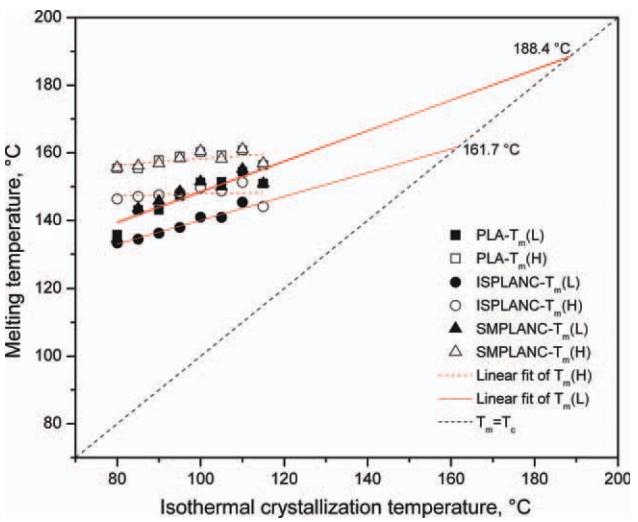

Figure 7 Melting temperatures of PLA and its nanocomposites as a function of isothermal crystallization temperature and Hoffman–Weeks analysis. [Color figure can be viewed in the online issue, which is available at wileyonlinelibrary.com.]

The values of T_m(L) and T_m(H) of PLA and its nanocomposites are plotted as a function of T_c in Figure 7. As can be observed clearly, T_m(L) increased continuously with increasing T_c in the evaluated temperature range, whereas T_m(H) remained almost unchanged. Increased T_m(L) indicated that the perfection and thickness of the growing PLA lamella crystals increased at higher T_c's.[20] PLA and SMPLANC exhibited nearly the same T_m(L) and T_m(H) at each T_c, whereas melting temperatures in the case of ISPLANC were much lower, suggesting thinner lamella crystals or defective crystalline regions in the nanocomposites in the presence of well dispersed TiO_2 nanowires. Many works on nanocomposites report a decrease of melting temperature compared with pristine polymers.[6,11,39,40] Two possible reasons explain the decreased melting temperatures of nanocomposites: One is that the mobility of polymer chains is greatly restricted by the nanoparticles in forming perfect and larger crystalline lamellar. Another is that the presence of the nanoparticles increases greatly the nucleation rate, whose characteristic time is much lower than the time required for chain disentanglement, thus disallowing the growth of well developed lamellar crystals.[40]

The equilibrium melting temperature can be measured by isothermal crystallization at various temperatures by carrying out a Hoffman–Weeks plot.[41,42] By fitting the data points of T_m(L) to a straight line (Hoffman–Weeks plot) and extrapolating it to $T_m = T_c$, the T_m^0 was determined (Fig. 7). PLA and SMPLANC showed the same T_m^0 of 188.4°C, whereas the T_m^0 of ISPLANC was much lower, only 161.7°C. The explanation for the T_m^0 reduction of ISPLANC was similar to that described above for melting temperatures.

CONCLUSIONS

In situ polymerization was a more effective approach than solution mixing in preparing PLA/TiO_2 nanowires nanocomposites. Crystallization growth rate first increased then decreased in the temperature range of 80–115°C, with maximum G_{exp} observed at 100°C. The TiO_2 nanowires acted as nucleation agents in the ISPLANC, which exhibited much higher G_{exp} than either pure PLA or SMPLANC below 110°C. But the ISPLANC had much smaller crystallization enthalpy at each T_c because of its restricted chain mobility in forming crystalline lamellar. The crystallization behavior of all the three samples fit the Avrami equation quite well. Double-melting behaviors were observed. The overall crystallinity of both PLA and nanocomposites increased in general as T_c increased in the evaluated temperature range. Equilibrium melting temperature of the ISPLANC was 161.7°C, and that of the SMPLANC was 188.4°C, same as PLA. The knowledge obtained about crystallization kinetics and melting behaviors of PLA and its nanocomposites could be useful references for optimizing the SSP process and designing PLA thermoplastics with desirable properties.

References

1. Drumright, R. E.; Gruber, P. R.; Henton, D. E. Adv Mater 2000, 12, 1841.
2. Jamshidian, M.; Tehrany, E. A.; Imran, M.; Jacquot, M.; Desobry S. Compr Rev Food Sci F 2010, 9, 552.
3. Lahiri, D.; Rouzaud, F.; Namin, S.; Keshri, A. K.; Valdes, J. J.; Kos, L.; Tsoukias, N.; Agarwal, A. ACS Appl Mater Interfaces 2009, 1, 2470.
4. Ray, S. S.; Bousmina, M. Porg Mater Sci 2005, 50, 962.
5. Wen, X.; Lin, Y.; Han, C.; Han, L.; Li, Y.; Dong, L. Macromol Mater Eng 2010, 295, 415.
6. Wu, C. S.; Liao, H. T. Polymer 2007, 48, 4449.
7. Zhang, J.; Lou, J.; Ilias, S.; Krishnamachari, P.; Yan, J. Polymer 2008, 49, 2381.
8. Gnanasekaran, D.; Madhavan, K.; Reddy, B. S. R. J Sci Ind Res 2009, 68, 437.
9. Kim, I.; Jeong, Y. G. J Polym Sci Part B: Polym Phys 2010, 48, 850.
10. Li, Y.; Sun, X. S. Biomacromolecules 2010, 11, 1847.
11. Nakayama, N.; Hayashi, T. Polym Degrad Stab 2007, 92, 1255.
12. Zheng, X.; Zhou, S.; Li, X.; Weng, J. Biomaterials 2006, 27, 4288.
13. Moon, S. I.; Lee, C. W.; Miyamoto, M.; Kimura, Y. J. J Polym Sci Part A: Polym Chem 2000, 38, 1673.
14. Moon, S. I.; Lee, C. W.; Taniquchi, I.; Miyamoto, M.; Kimura, Y. Polymer 2001, 42, 5059.
15. Moon, S. I.; Taniquchi, I.; Miyamoto, M.; Kimura, Y.; Lee, C. W. High Perform Polym 2001, 13, S189.
16. Iannace, S.; Nicolais, L. J Appl Polym Sci 1997, 64, 911.
17. Wu, D.; Wu, L.; Wu, L.; Xu, B.; Zhang, Y.; Zhang, M. J Polym Sci Part B: Polym Phys 2007, 45, 1100.
18. Kawai, T.; Rahman, N.; Matsuba, G.; Nishida, K.; Kanaya, T.; Nakano, M.; Okamoto, H.; Kawada, J.; Usuki, A.; Honma, N.; Nakajima, K.; Matsuda, M. Macromolecules 2007, 40, 9463.
19. Tsuji, H.; Nakahara, K.; Ikarashi, K. Macromol Mater Eng 2001, 286, 398.
20. Krikorian, V.; Pochan, D. J. Macromolecules 2004, 37, 6480.
21. Nam, J. Y.; Ray, S. S.; Okamoto, M. Macromolecules 2003, 36, 7126.
22. Papageorgiou, G. Z.; Achilias, D. S.; Nanaki, S.; Beslikas, T.; Bikiaris, D. Thermochim Acta 2010, 511, 129.
23. Shieh, Y. T.; Liu, G. L. J Polym Sci Part B: Polym Phys 2007, 45, 1870.
24. Li, Y.; Chen, C.; Li, J.; Sun, X. S. Polymer 2011, 52, 2367.
25. Zhang, Y. X.; Li, G. H.; Jin, Y. X.; Zhang, Y.; Zhang, J.; Zhang, L. D. Chem Phys Lett 2002, 365, 300.
26. Fischer, E. W.; Sterzel, H. J.; Wegner, G. Kolloid-ZuZ Polym 1973, 251, 980.
27. Fraïsse, F.; Nedelec, J. M.; Grolier, J. P. E.; Baba, M. Phys Chem Chem Phys 2007, 9, 2137.
28. Huang, C. I.; Tsai, S. H.; Chen, C. M. J Polym Sci Part B: Polym Phys 2006, 44, 2438.
29. Supaphol, P. Thermochim Acta 2001, 370, 37.
30. Avrami, M. J Chem Phys 1939, 7, 1103.
31. Avrami, M. J Chem Phys 1940, 8, 212.

32. Avrami, M. J Chem Phys 1941, 9, 177.
33. Lorenzo, A. T.; Arnal, M. L.; Albuerne, J.; Muller, A. J. Polym Test 2007 2007, 26.
34. Liao, R.; Yang, B.; Yu, W.; Zhou, C. J Appl Polym Sci 2007, 104, 310.
35. Mano, J. F.; Wang, Y.; Viana, J. C.; Denchev, Z.; Oliveira, M. J. Macromole Mater Eng 2004, 289, 910.
36. Zhang, J.; Tsuji, H.; Noda, I.; Ozaki, Y. Macromolecules 2004, 37, 6433.
37. Wunderlich, B. Macromolecular Physics; Academic: New York, 1980; Vol.3.
38. Yasuniwa, M.; Tsubakihara, S.; Sugimoto, Y.; Nakafuku, C. J Polym Sci Part B: Polym Phys 2004, 42, 25.
39. Hao, J.; Yuan, M.; Deng, X. J Appl Polym Sci 2002, 86, 676.
40. Maio, E. D.; Iannace, S.; Sorrentino, L.; Nicolais, L. Polymer 2004, 45, 8893.
41. Hoffman, J. D.; Weeks, J. J. J Chem Phys 1965, 42, 4301.
42. Weeks, J. J. J Res Nat Bur Stand 1963, 67A, 441.